A COMPARATIVE FINITE ELEMENT STUDY OF CUBIC UNIT CELLS FOR SELECTIVE LASER MELTING

A.O., Aremu, I. Maskery, C. Tuck, I. A., Ashcroft, R.D., Wildman, and R.I.M, Hague

EPSRC Centre for Innovative Manufacturing in Additive Manufacturing, Faculty of Engineering, University of Nottingham, Nottingham, NG7 2RD, UK.

REVIEWED

Abstract

Selective laser melting (SLM) enables the utilization of complicated lattice structures in metallic components. To exploit this capability, it is important to understand the structural properties of these lattices. Topological variations in lattices are diverse, however, only a few are suitable for SLM since some lattices require supports during manufacture while others self-support. Difficulties associated with the removal of these supports and their detrimental effects on surface finish makes the latter group better suited for SLM. In this work, we investigate the structural properties of some self-supporting unit cells via a finite element study and show that the performance of a lattice structure is largely dependent on the topology of the unit cell. Variants of the gyroid and face centred cubic unit cells performed better than body centred cubic cells. This was also observed when lattices, made of repeating unit cells were compared.

1 Introduction

Additive manufacturing (AM) techniques for metals could improve the mechanical performance of components, since they are less reliant on constraints imposed by traditional techniques. However, ideas are needed to overcome barriers encountered with AM for metals. The need for supports during manufacture is a prevalent issue as this has a detrimental effect on the surface finish [1]; and in some cases, where the topology of the component is highly complex, such supports are difficult to remove. Support structures are used to preserve the structural integrity of a component experiencing thermal stresses during manufacture [2]. By suitably orientating the component, the problem can be mitigated, yet supports are required to separate the component from the build platform. Restricting supports to accessible regions of a component's domain is beneficial. This is particularly useful when selective laser melting (SLM) is used to produce components embedded with lattice structures, removing supports from lattices is impractical.

There is a growing interest in understanding the structural properties of lattices produced with SLM. The build chamber, laser settings and morphology of the powder could affect the quality of the lattices, however, it is the choice of material, topology and relative density of the lattice that greatly influence structural properties [3]. Materials development for SLM is an active area of research with stainless steel, titanium and nickel alloys being used for lattices as seen in [4, 5, 6, 7]. Hasan et al. [6] observed that heat treating a body centered cubic (BCC) lattice composed of a titanium alloy improved it microstructural properties while dispersing contaminates. Gumrik and Mines [7] studied the BCC

lattice and proposed a theoretical model for the compressive behaviour of the lattice with stainless steel as the base material. Stainless steel was also employed by Yan and Hao [8] to understand the dependence of the structural properties of gyroid lattices on the cell size. The effective yield strength and modulus of the gyroid were observed to decrease as the cell size increased. Smith and Guan [9] studied the BCC lattice and its variant, the $BCCz$, and observed that the stiffness and yield strength of the lattices significantly improved when the aspect ratio of the unit cell was reduced.

Gyroid and BCC lattices and some of their variants require no supports and have therefore been studied extensively. However, there is a broader class of self-supporting lattices with potentially better structural properties. Also, Thomas [2] outlined design rules to achieve self-supporting designs. This creates an opportunity to develop lattices for SLM, yet it is important to understand the structural benefits of existing lattices. In this paper, the stiffness of the BCC, face centered cubic (FCC) and gyroid lattices are compared via finite element analysis.

2 Self-supporting Unit cells

Triangilar facets were generated to define the topology of seven self-supporting cubic unit cells. The length, width and height of cell was set to 10 mm. Facets were subsequently written into STL files with relative density, 0.23, to ensure a fair comparison can be made across the cells. The relative density is the ratio of the density of the cell to that of a solid cube with same dimensions. The structural stiffness of seven self-supporting unit cells was then determined and compared. Cells include variants of BCC, FCC and gyroid lattices as seen in Fig. 1. The BCC cell is composed of eight cylindrical struts which connect the center of a cube to its corners and trimmed to fit the cube (Fig. 1a). Constituent members of the cell are inclined to the x-y plane at 45° which is the minimum angle for self supporting members as observed by Thomas [2]. The structural stiffness of the BCC cell along the z axis improves by adding four vertical struts to the cell. The struts connect upper corners of the cell to the lower and transforms the topology into a $BCCz$ cell as seen in (Fig. 1b). The $BCCz$ cell is self-supporting only if the angle between the build platform and all constitutent members is greater than 45°. The gyroid cell shown in Fig. 1c represents a minimal surface proposed by Schoen [10]. For a three dimensional Cartesian coordinate space x, y, z, the gyroid surface conforms to the equation:

$$sin(\frac{2\pi}{L}x)cos(\frac{2\pi}{L}y) + sin(\frac{2\pi}{L}y)cos(\frac{2\pi}{L}z) + sin(\frac{2\pi}{L}z)cos(\frac{2\pi}{L}x) - t = 0 \qquad (1)$$

where L is the size of the cube and t is a constant parameter. t assumes a value between 0 and 1.413. A variant of the gyroid, shown in Fig. 1d is the matrix form of the double gyroid (D-gyroid) [11]. The equation for this cell is derived from Eqn. 1 by squaring it's three terms. Eqn. 1 becomes:

$$(sin(\frac{2\pi}{L}x)cos(\frac{2\pi}{L})y + sin(\frac{2\pi}{L}y)cos(\frac{2\pi}{L})z + sin(\frac{2\pi}{L}z)cos(\frac{2\pi}{L}x))^2 - t^2 = 0 \qquad (2)$$

FCC includes members that connect the corners of the cube to the center of faces perpendicular to the x-y plane. $PFCC$ is a variant of FCC with four vertical struts to improve stiffness along the z axis. F_2BCC is a boolean combination of BCC and F_2BCC.

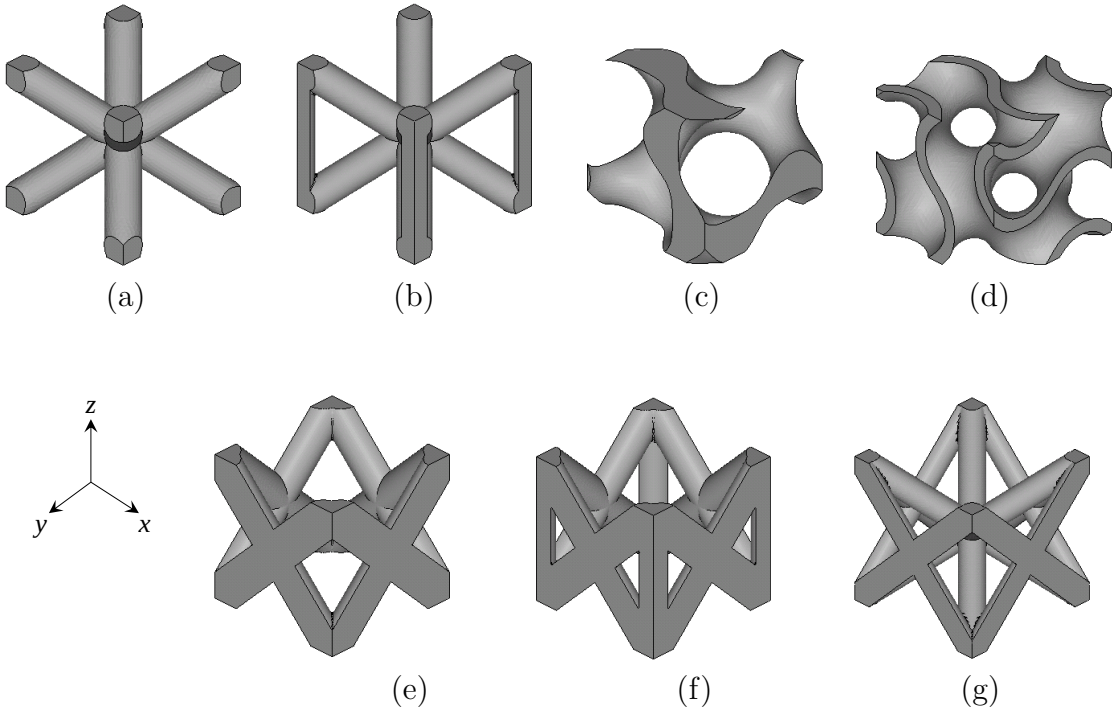

Figure 1: Seven self-supporting unit cells: (a) BCC (b) $BCCz$ (c) Gyroid (d) matrix phase of D-gyroid (e) FCC (f) $PFCC$ (g) F_2BCC.

3 Finite Element Convergence Study

Preliminary studies were performed to determine cellular parameters require to set the relative density of STL files at 0.23. The relative densities of BCC, $BCCz$, FCC, $PFCC$ and F_2BCC were controlled by the radius, R, of the cylindrical members. Members within a cell were constrained to share the same R which was then varied iteratively until the target density was achieved. The resultant values for R are shown in Table 1. R is clearly dependent on the number of members, M, and the length of these members. For the gyroid lattices, t was varied in Eqn 1 and 2 until the relative density constraint was achieved. A lower value of t was determined for D-gyroid than that for the gyroid as shown in Table 1. For the first set of FEA simulations, STL models of the unit cells were voxelized and converted to hexahedral meshes. Voxelization is the conversion of a model represented by surfaces or patches into a bitwise three dimensional array. The array contains the value one in regions enclosed by the STL and zero in unoccupied regions. Methods for voxelizing STL models and other triangular facets can be found in [12, 13, 14]. Each voxel enclosed an integral portion of the cells domain with a shape that largely resembles that of a hexahedral element. Therefore, regions of the voxel array holding a value of one were mapped directly into an hexahedral mesh as illustrated in Fig. 2 for the D-gyroid cell. The resolution of the voxels was used to control the mesh size during convergence studies. By increasing the resolution of voxels, more hexahedral elements are introduced in the mesh until convergence was reached. Convergence was achieved once the change in maximum displacement along the loading axis was less than 1% for 100% increase in the number of elements. The meshing strategy preserved the quality of elements and avoided numerical errors associated with distorted elements.

Table 1: Parametric values R and t for the unit cells used to set relative density to 0.23.

Unit Cell	BCC	$BCCz$	Gyroid	D-gyroid	FCC	$PFCC$	F_2BCC
R (mm)	1.15	1.08	-	-	1.29	1.20	0.86
t	-	-	0.91	0.36	-	-	-
M	8	12	-	-	16	20	24

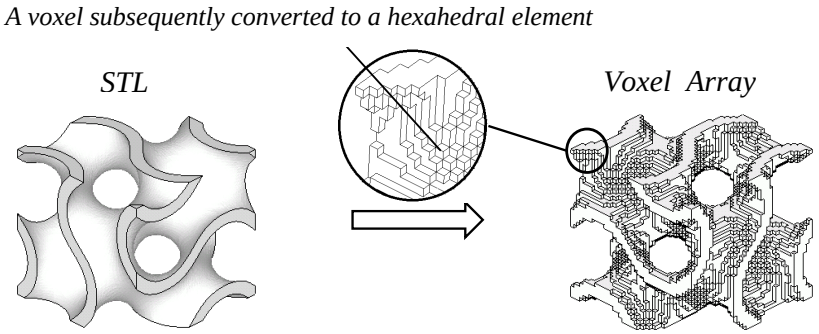

Figure 2: Conversion of D-gyroid STL to voxel array.

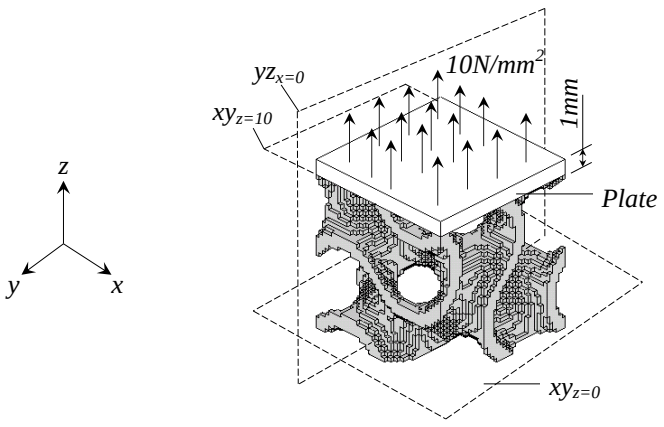

Figure 3: Pressure loading on a D-gyroid cell.

A set of hexahedral elements constituting a 1 mm thick plate was placed on the cells along the z-axis, on Plane $xy_{z=10}$. The plate experienced a tensile pressure of 10 N/mm^2 on it upper face as illustrated in Fig. 3. Nodes on Plane $xy_{z=0}$ were fixed for both translational and rotational degrees of freedom. The Young's modulus of elements associated to the unit cell was set to 100 GPa and Poission ratio was 0.342 which typical for SLM compatible metals. Plate elements assumed material properties that was many times stiffer than the cell elements. A static linear structural analysis was performed and the mesh was progressively refined until convergence was achieved. The plate was later rotated so that the pressure on it's face aligned with the x-axis. Nodes on the Plane $yz_{x=0}$ were fixed for all degrees of freedom and the lower face of the plate was located at Plane $yz_{x=10}$ which is the farthest face of the cell along the x-axis. The convergence simulations was then repeated for this boundary condition.

A second set of simulations was performed to investigate if observed differences across the cells translates to their lattices. Lattice structures were generated for the cells by tessellating their voxel arrays as proposed in [15]. The length, width and height of each lattice was set to 40 mm while the unit cell size remained at 10 mm resulting in a 4 by 4 by 4 lattice. This is illustrated for the D-gyroid in Fig. 4. To improve computational efficiency, a quarter of the lattice was modelled and symmetrical constraints were imposed along the planes of symmetry. This is an established way of reducing large FEA model which gives the same results as the full model.

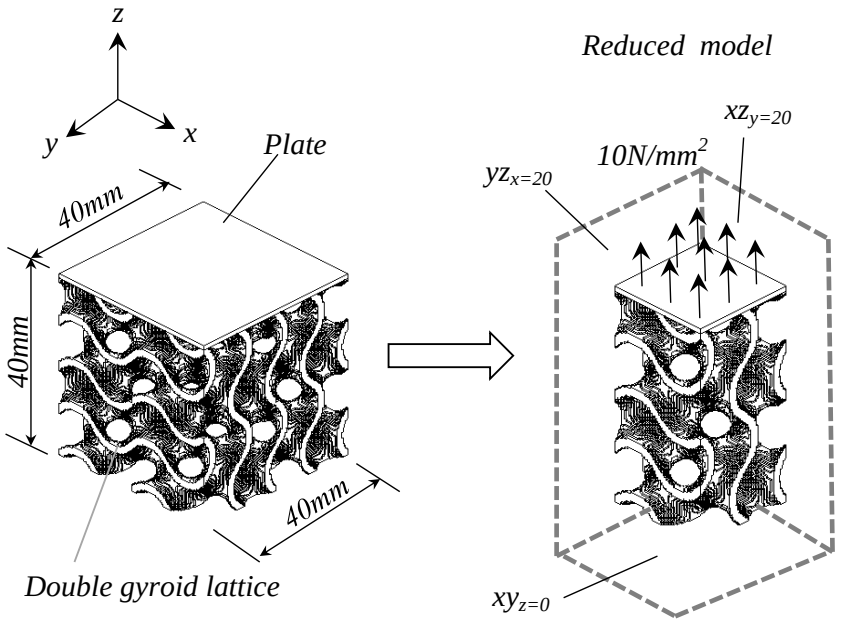

Figure 4: Constructing reduced FEA models for the D-gyroid lattice.

This was achieved by diving the full model along centric Plane $yz_{x=20}$ and $xz_{y=20}$ and elements in one of the four quadrants were retained. Nodes residing on $yz_{x=20}$ were fixed along x-axis while those on the $xz_{y=20}$ were fixed along the y axis. Nodes on $xy_{z=0}$ were fixed for all degrees of freedom and the upper face of the plate experienced a pressure of 10 N/mm^2. Simulations were repeated for pressure loads along the x-axis with sectional Plane $xy_{z=20}$ and $xz_{y=20}$ used to reduce the FEA model.

4 Results

Displacement along z and x axes due to pressure loads are plotted against the number of elements in Fig. 5. Fig. 5a shows results for z-axis while those for x-axis are shown in Fig 5b.

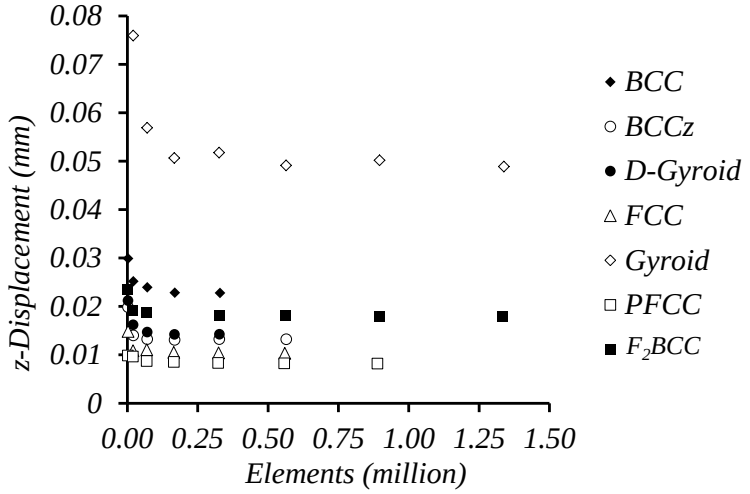

(a)

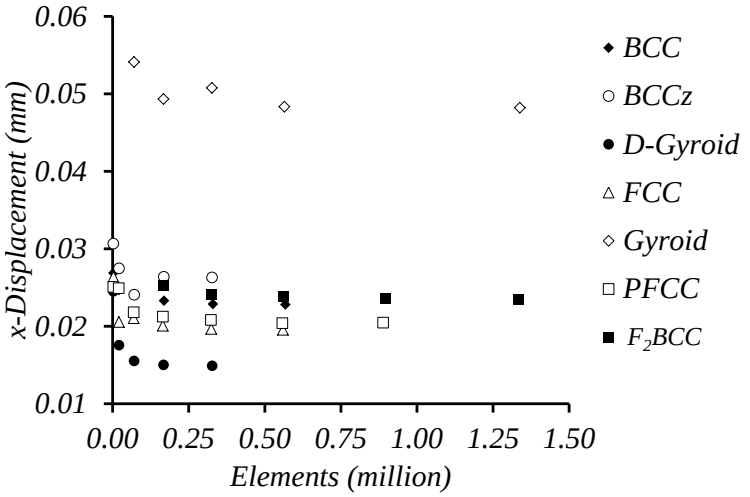

(b)

Figure 5: Finite element convergence plot for the unit cells (a) z-displacements (b) x-displacements.

The following is deduced from the scattered plots:

- The gyroid cell reached the greatest displacement for both the z and x axes suggesting it the weakest of the cells,
- BCC has the second largest displacement along the z-axes but lower than three other cells along the x-axis,
- The D-gyroid cell achieved the lowest displacement along the x and competively lower displacement along the z-axis
- Displacement for FCC and $PFCC$ cells along both axis are lower than most of the other cells,

Convergence plot for the Lattices are shown in Fig. 6.

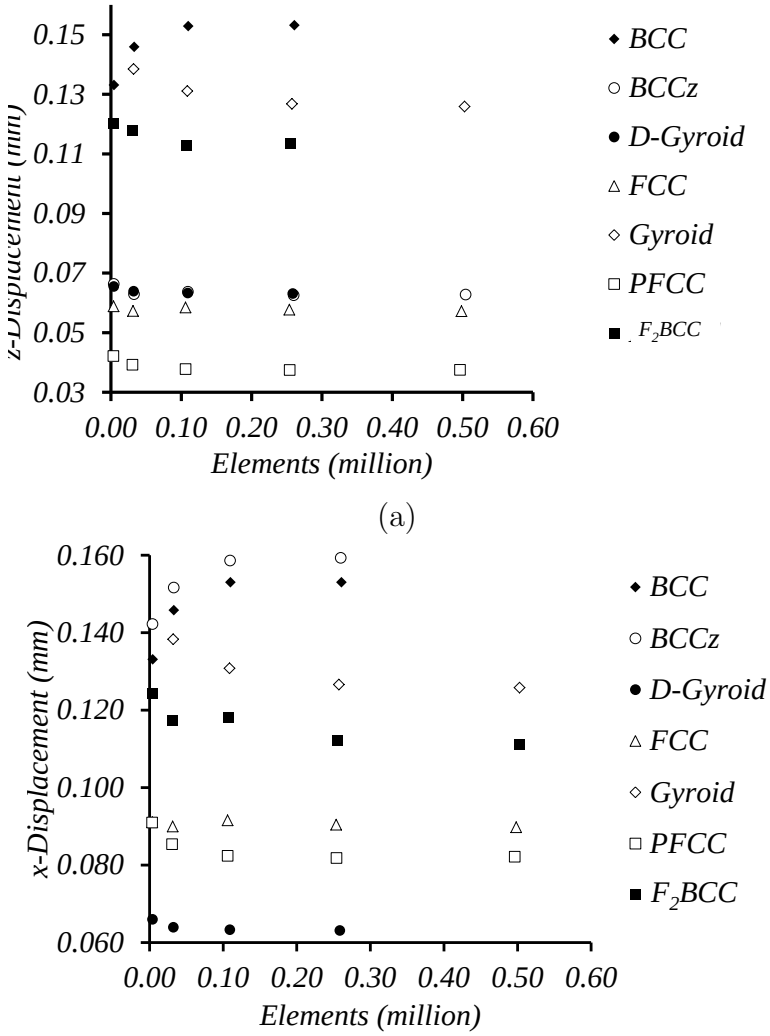

Figure 6: Finite element convergence plot for the lattices (a) z-displacements (b) x-dizplacements.

Displacement for the lattices are generally higher than those for the cells which is consequence of a greater force on the lattices. Comparing the scattered plots for the lattices with those for the cells, it is observed that:

- D-gyroid lattice achieved the lowest displacement in the x-axis,
- Displacement for FCC and $PFCC$ cells along both axis are lower than most of the other cells,
- The D-gyroid lattice has similar stiffness to that of $BCCz$ in the z-axis but approximately two times stiffer than $BCCz$ in the x-axis,
- The gyroid lattice is better than the BCC lattice in x and z axes,

The first three observation are consistent with those of the cells, however, the fourth contradicts deduction from the comparision of the BCC and gyroid cells. This suggests that the properties from both cells is insufficient to determine the performance of the BCC and gyroid lattices. Also, the presence of the vertical members in the $BCCz$ only improves the stiffness of the lattice along the z and has no effect in the x since $BCCz$ is weaker than BCC along the x-axis.

5 Discussion

The stiffness, K of the unit cells and lattices was determined as the ratio of total force on the plate to the maximum displacement along an axis. Mathematically,

$$K = \frac{PA}{d} \tag{3}$$

where P is the pressure on the plate and assumes a value of 10 N/mm^2 and A is the surface area of the plate. d is the converged maximum displacement along either of the two axis. For the cells, A is 100 mm^2 while for the lattice it is estimated to be 1600 mm^2. K along z and x axes for cells and lattices are plotted as bar charts and shown in Fig. 7.

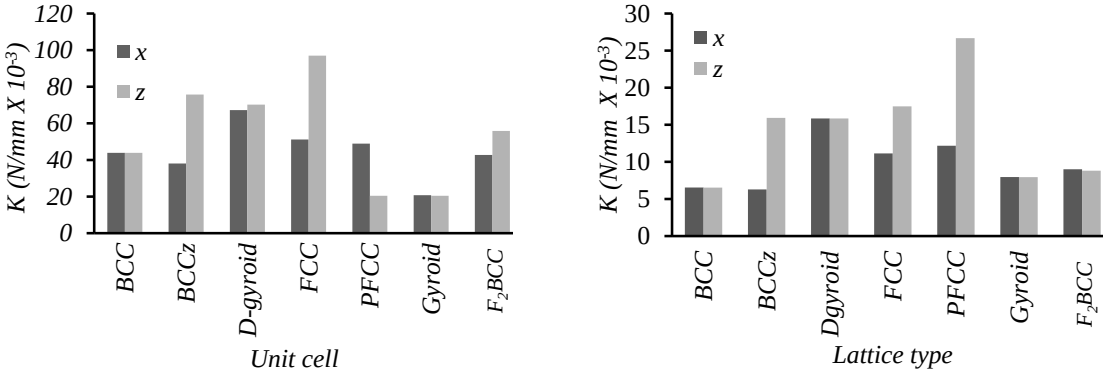

Figure 7: Maximum stiffness for the cells (a) Lattice (b).

BCC, D-gyroid and gyroid cells and lattices have approximately similar K along both z and x axes. This could be attributed to their cubic symmetric properties. The F_2BCC lattice also show similar behaviour in both z and x axes (Fig. 7b), this is not evident for the F_2BCC cell (Fig. 7a). Also, $BCCz$, FCC, and $PFCC$ showed contrasting stiffness in the axes. Observed peak stiffness for the lattices is exhibited by $PFCC$ along the $z-$axis which is a consequence of the minimal displacement in this axis. However, $PFCC$ stiffness along the x-axis is approximately 30% lower than that for D-gyroid. The maximum von Mises stresses for cells and lattices are shown in Fig. 8.

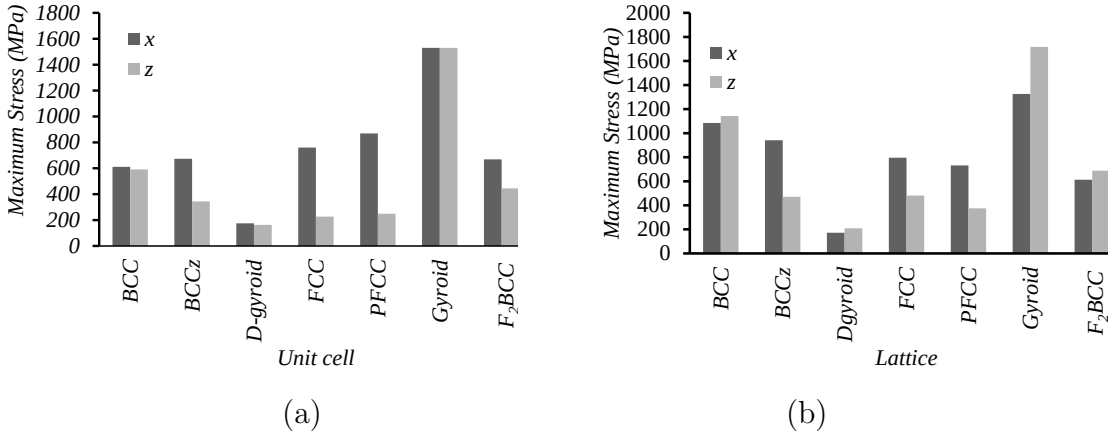

Figure 8: Maximum stresses for cells (a) lattices (b).

The D-gyroid lattice and cell exhibit the lowest stress in both axes. It's variant, the gyroid, performs the worst achieving stresses many times greater than that of the D-gyroid. Again, both D-gyroid and BCC show similar stress levels in both axes, however, maximum stresses in the D-gyroid are a fraction of those in BCC. Stress levels in $PFCC$ and FCC along the z-axis is better that in the x-axis. $PFCC$ and FCC was seen to have greater stiffness along the z-axis than those of D-gyroid, however, stresses in their cell and lattice are much larger as seen Fig. 8a and 8b.

For structural applications involving pressure loads along a single axis, FCC or $PFCC$, is better than the other five types. It is common for components to experience multiple pressure loads in different orthogonal axes, it is therefore preferrable to utilize a lattice that shows superior performance in more than one axis. For this instance, the D-gyroid lattice is better than the other lattices since it acheived competitive stiffness in both z and x axes with lower stresses. The behaviour of the cells and lattices have not been determine for pressure loads along the y-axis since this can be deduced from observations in z and x axes. BCC, $BCCz$, FCC, $PFCC$ and F_2BCC are symmetrical about centric zy planes, implying that their behaviour along the y-axis is largely similar to those in the x-axis if the similar pressure loads were applied in both axes. Both gyroid and D-gyroid are not symmetric about the centric zy planes, however, they do exhibit cubic symmetric properties as described by Scherer [11]. It was seen that their stiffness is largely similar in both z and x axes. Therefore, properties of both lattices along y-axis would be similar to those observed in z or x. Superior qualities of the D-gyroid lattice automatically translates to the y-axis.

Thermostructural applications of lattices are common. These have not been considered in this work, however, the relative thermal dissipative and insulative properties of the cells is in principle deducible from their total surface areas. The surface areas of the cells are plotted in Fig. 9.

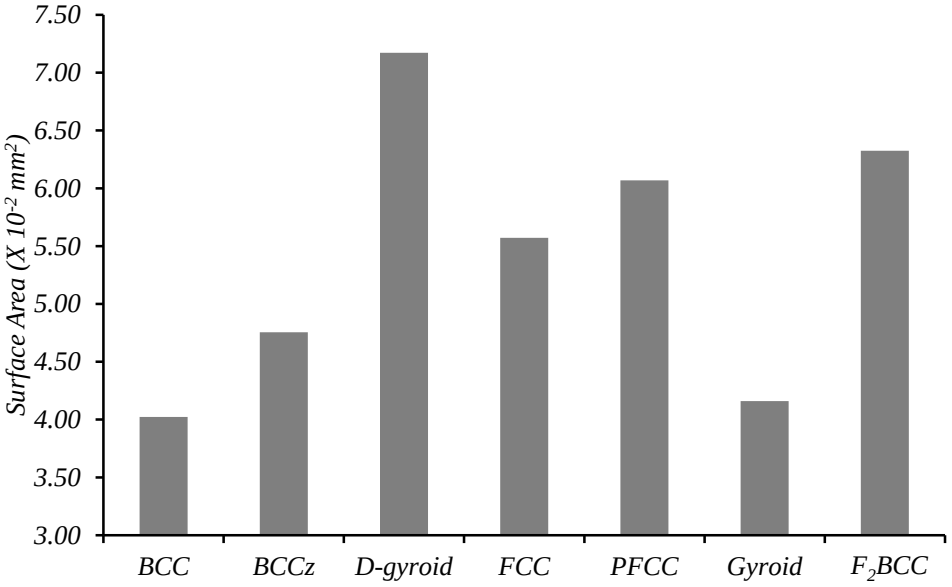

Figure 9: A comparison of surface area of the unit cells with similar density.

It can be seen that the D-gyroid lattice has the greatest surface area, suggesting it has the greatest capacity to dissipate heat when a cooling agent is flushed across it's surface. F_2BCC also show some capacity to dissipate heat in since it has a greater surface area than either BCC, $BBCz$, FCC, $PFCC$ and gyroid; therefore, there is greater interaction between the agent and F_2BCC surfaces. For applications where thermal insulation is paramount, the BCC and the gyroid lattice are better since they have the least capacity to transport heat owing to their relative low surface areas. However, surface defects would propagate faster on D-gyroid and F_2BCC since they include thinner members in a broader space.

6 Summary and Conclusions

The capabilities of SLM is evident for metallic components since a wider range of topologies can be realized as opposed to traditional techniques. However, most would require support structures to prevent warping and curling of the part during the build, while other would self-support. Difficulties associated with removing these supports makes self-supporting solutions more suited for SLM. Supports are particularly difficult to remove from lattices, therefore it is preferrable to design latticed components that reduce the need for supports. Interestingly, a number these lattices exist, some of which have previously been characterized with SLM. In this work, the structural stiffness and stresses in BCC, $BCCz$, FCC, $PFCC$, D-gyroid, F_2BCC and gyroid cell and lattices were compared. To ensure a fair comparison is made across the lattices and cells, the relative density for cells was fixed at 0.23. The FCC, $PFCC$ and D-gyroid lattices were found to exhibit superior perfomance to those of the other lattices. Also, the D-gyroid cell

has the greatest surface area implying that it has a better potential to dissipate heat if it's interact with a cooling agent. *BCC* and gyroid lattice are poorest at dissipating heat owing to their relatively low surface area and can potentially be used as a thermal insulator. The choice of lattice is largely dependent its application.

7 Acknowledgements

This work is funded by the engineering and physical science research council (EPSRC) and the technology strategy board (TSB).

References

[1] Strano, G., Hao, L., Everson, R., M., Evans, K., E., *A new approach to the design and optimisation of support structures in additive manufacturing*, Int J Adv Manuf Technol, 66, p1247-1254, 2013.

[2] Thomas, D., *The development of design rules for selective laser melting*, PhD dissertation, University of Wales, Cardiff, 2009.

[3] Ashby, M., F., *The properties of foams and lattices*, The Royal Society: Mathematical physical and engineering sciences, 68, p17, 2006.

[4] Yan, C., Hao, L., Hussein, A., Young, P., Raymont, D., *Advanced lightweight 316L stainless steel cellular lattice structures fabricated via selective laser melting*, materials and Design, 55, p533-541, 2014.

[5] Hakan, B., Saarimaki, J., *Mechanical properties of lattice truss structures made of a selective laser melted superalloy*, 13th international conference on fracture, Beijing, p10, 2013.

[6] Hasan, R., Mines, R., Fox, P., *Characterization of selective laser melted Ti-6Al-4 V micro lattice struts*, Procedia Engineering, 10, p536-541, 2011.

[7] Gumruk, R., Mines, R., A., W., *Compressive behaviour of stainless steel micro-lattice structures*, International Journal of Mechanical Sciences, 68, p125-139, 2013.

[8] Yan, C., Hao, L., Hussein, A., Young, P., Raymont, D., *Evaluations of cellular lattice structures manufactured using selective laser melting*, International Journal of Machine Tools and Manufacture, 62, p32-38, 2012.

[9] Smith, M., Guan, Z., Cantwell, W., J., *Finite element modelling of the compressive response of lattice structures manufactured using the selective laser melting technique*, International Journal of Mechanical Science, 67, p28-41, 2013.

[10] Schoen, A., H., *Infinite periodic minimal surfaces without self-intersections*, NASA Technical Note D-5541, 1970.

[11] Scherer, M., R., J., *Double-Gyroid-Structured Functional Materials*, Springer Theses, DOI:10.1007/978 − 3 − 319 − 00354 − 2_2, Springer International Publishing Switzerland, 2013.

[12] Karabassi, A., Papaioannou G., Theoharis, T., *A depth duffer based voxelization algorithm*, Journal of Graphics Tools, 4(4), p. 5-10, 1999.

[13] Fang, S., Chen, H., *Hardware accelerated voxelization*, Volume Graphics, p. 301-315, 2000.

[14] Thon, S., Gesquiere, G., Raffin, R., *A Low cost anatialiased space filled voxelization of polygonal objects*, International Conference Graphion, 2004.

[15] Brennan-Craddock, J., P., J., *The investigation of a method to generate conformal lattice structures for additive manufacturing*, PhD thesis, Loughborough University, 2011.